Keck Adaptive Optics Note (KAON) 497

NGAO High-Contrast & Companion Sensitivity Performance Budget (WBS 3.1.1.10)

Ralf Flicker[a], Bruce Macintosh[b], Richard Dekany[c], Michael Liu[d], Christopher Neyman[a]

(a) W. M. Keck Observatory, 65-1120 Mamalahoa Hwy., Kamuela, HI 96743
(b) Lawrence Livermore National Laboratory, 7000 East Avenue, Livermore, CA 94550
(c) Caltech Optical Observatories, California Institute of Technology, Pasadena, CA 91125
(d) University of Hawai'i, 2680 Woodlawn Drive, Honolulu, HI 96822

27 June 2007

1 Introduction

This text addresses Next Generation Adaptive Optics (NGAO) performance budget topics pertaining to the subset of NGAO science cases that depend more heavily on specific PSF qualities, such as a local contrast metric, than it does on the overall wavefront error. Those science cases include detection of faint companions (planets, brown dwarfs) and imaging of debris disks and proto-stellar envelopes around nearby stars. Two different analysis tools are used in order to assess the capabilities of certain NGAO system configurations to meet the science requirements for these science cases. One part of the analysis is carried out by an analytical tool that computes a local contrast metric based on a Fourier domain modeling of residual power spectral densities (PSDs) of the adaptive optics (AO) wavefront. The second part of the analysis is done by a numerical AO simulation tool that produces long-exposure point spread functions (PSFs) by averaging over many cycles of random turbulence phase screens. The details of these tools are elaborated in later sections of the text.

2 High-contrast imaging

2.1 Contrast metrics

Various types of science scenarios may be advantageously described and analyzed by different types of image quality metrics. For quantifying the performance of partially compensated adaptive optics (AO) images the Strehl Ratio (S) can be a useful indicator. For seeing-limited imaging the Strehl Ratio is not a very good metric, however, as it has rather poor sensitivity at very low values, and a full-width at half maximum (FWHM) measure is usually used instead. Somewhere in between these two extremes, an image contrast ratio $C_p = S/(S + 2S_H)$ is sometimes used [1], where S_H is the normalized peak intensity of the halo. C_p is more sensitive to image quality variations at low Strehls, but it saturates to unity more quickly than S at high Strehl Ratios. S_H refers to a simplistic core-halo model of the AO PSF, see Fig. 1 (left hand graph), where the AO PSF morphology is entirely described by the relative strength and width of two components, a central coherent core and a diffuse halo of scattered light. Global image metrics such as S, C_p and the FWHM may be useful in quantifying the large scale angular resolution and the ability of the AO system to separate sources that are within a few magnitudes of each other in a crowded field.

These metrics are of limited use, however, in determining the ability to detect a faint source in the halo of a much brighter star. In this case, the detection threshold depends more strongly on local small-scale brightness variations in the PSF halo, at the position of the faint companion, as is evident from inspection of some more realistic PSF models in Figs. 1 (right) and Fig. 2. If the halo of the primary (host) star was perfectly smooth, a faint companion (secondary) could be detected as a deviation against a (nearly) flat background. It becomes necessary to define a

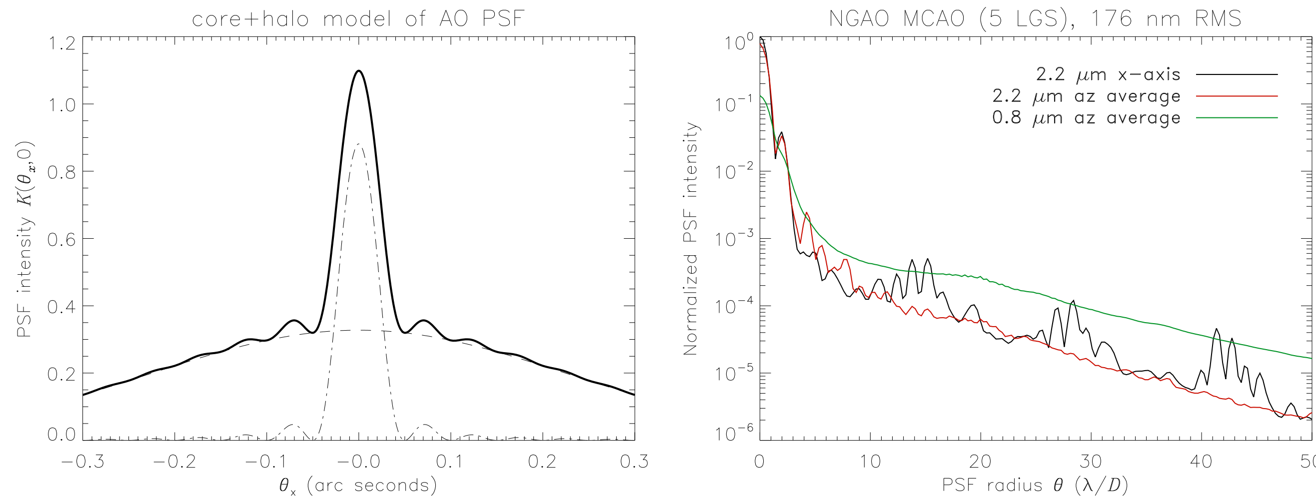

Figure 1: AO PSF morphology and contrast definition issues. Top left: core+halo model of partially compensated AO PSF (arbitrary parameters, for illustration only, not adjusted to NGAO parameters). Top right: example azimuthal average and x-axis cross-section PSF profiles from numerical AO simulations of a typical NGAO configuration.

local contrast metric that is a function of the angular position in the PSF. One possible such metric is given by

$$C_{\mathcal{A}}(\theta_x, \theta_y) = \frac{\sqrt{\langle K^2(\theta_x, \theta_y)\rangle_{\mathcal{A}}}}{K(0,0)}, \tag{1}$$

where $K(\theta_x, \theta_y)$ is the PSF and $\{\theta_x, \theta_y\}$ are the angular two-dimensional rectangular coordinates in the image plane, and $\langle\cdot\rangle_{\mathcal{A}}$ denotes averaging over the aperture $\mathcal{A}$. The measurement $C_{\mathcal{A}}$ is thus a normalized standard deviation over the (small) aperture $\mathcal{A}$. To simplify the presentation we can without much loss of generality compress one dimension of $C_{\mathcal{A}}$ by computing its azimuthal average $C(\theta) = \langle C_{\mathcal{A}}(\theta_x, \theta_y)\rangle_\psi$, where $\{\theta, \psi\}$ are the polar components of $\{\theta_x, \theta_y\}$ according to $\theta^2 = \theta_x^2 + \theta_y^2$ and $\tan\psi = \theta_y/\theta_x$. Hence θ is the radial distance from the center of the PSF, and $\langle\cdot\rangle_\psi$ denotes averaging over the azimuthal direction – we will henceforth be referring to the quantity $C(\theta)$ as the essential contrast measurement of interest. In some cases it is also instructive to look at the direct core-halo contrast defined as $C_0(\theta) = \langle K(\theta_x, \theta_y)\rangle_\psi / K(0,0)$, which is simply equivalent to the normalized azimuthal average of the PSF (two of the curves plotted in the right hand graph of Fig. 1 are of this kind).

2.2 Observing scenarios

The key observing scenarios relevant to NGAO high-contrast analysis are described in the Science Case Requirements Document (SCRD) KAON 455 and are not repeated here. The science cases for planets around low-mass stars place some of the most demanding constraints on AO performance and calibration of static errors, so we will take those as benchmark goals initially in this study. The non-coronagraphic science cases center on asteroid detection and characterization. From the System Requirements Document (SRD) KAON 456, various levels of requirements for this science case are given by:

1. ΔJ $= 10$ at $0.2''$. 15 AU cutoff – 20 to 30 pc; distribution peaks at 4 AU $= 0.2''$ which allows 2 $M_{\rm Jup}$
2. a) ΔJ $= 8.5$ at $0.1''$ minimum; b) ΔJ $= 11$ at $0.2''$ nominal; c) ΔJ $= 11$ at $0.1''$ goal
3. ΔJ $= 13.5$ at $0.07''$. Placeholder at 5 Myr, 1 $M_{\rm sun}$ primary; goal ΔJ $= 13.5$ for 1 $M_{\rm Jup}$ or ΔJ $= 9$ for 5 $M_{\rm Jup}$
4. ΔH ≥ 5.5 at $0.5''$ for a $V \geq 17$ asteroid $< 2''$
5. ΔI ≥ 7.5 at $0.75''$ for a $V \geq 17$ asteroid $< 2''$

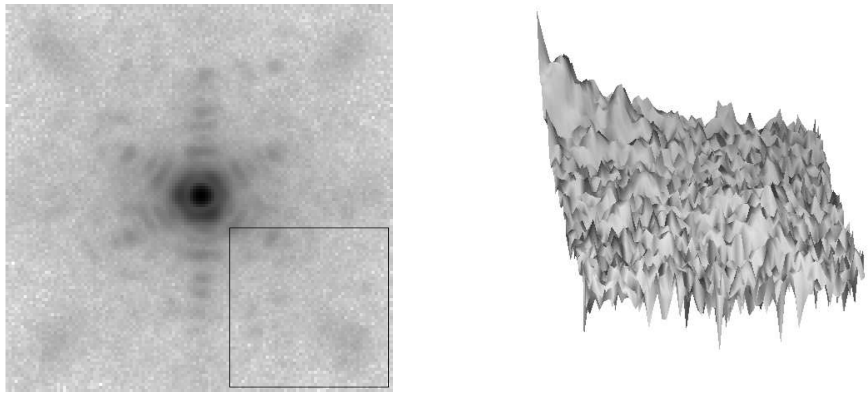

Figure 2: Sample long-exposure NGAO PSF from AO simulation, with the lower right quadrant magnified in the surface graph to the right, illustrating the effects of local brightness variations due to atmospheric and static speckles, and photon/detector noise. It is clear that the overall Strehl Ratio or wavefront error as performance metrics have little relevance to planet-detection abilities in such a locally noisy environment. Both images are stretched by an inverse hyperbolic sine (asinh).

The science requirements are formulated in terms of delta-magnitudes Δm which refer to the apparent magnitude difference between the primary (host) and secondary (companion) source. These will be referred to as science goals 1-5 respectively, where 1-3 require the use of a coronagraph instrument, and 4-5 are done with pure AO (but comes with additional constraints on tracking accuracy, see the SRD).

2.3 Coronagraphic imaging

A coronagraph straw man concept has not yet been developed for NGAO. For this first round of high-contrast analysis, a generic apodized Lyot type coronagraph (ApLC) of the type described in e.g. [4] was used in the numerical AO simulations that employed a coronagraph, somewhat adapted for the hexagonal pupil shape of the Keck primary mirror. A sketch of its function and the corresponding diffraction-limited images and pupils are shown in Fig. 3. The occulting spot in the first focal plane was varied from $6\lambda/D$ to $14\lambda/D$, where D is the telescope diameter and the imaging wavelength λ ranged between 0.7μm to 3.5μm. The on-axis throughput of the coronagraph was measured on the primary star (i.e. the guide star) during the simulations in order to normalize the PSFs to the proper photometry for the simulated observing scenarios, see table 1. Post-processing methods and speckle suppression strategies are not addressed in detail in this first version of the report, although it is acknowledged in the SRD that the coronagraph instrument may be equipped with dual- or multi-channel modes for speckle suppression and rejection of background objects by differential imaging. A simple method to account for speckle suppression techniques is included in the analytical contrast spread sheet tool (introduced in the next section), and its consequences are examined briefly.

OCCULTING SPOT SIZE	WAVELENGTH BAND R	I	J	H	K	L
$6\lambda/D$	0.435	0.267	0.188	0.114	0.068	0.029
$10\lambda/D$	0.365	0.218	0.151	0.092	0.054	0.023
$14\lambda/D$	0.306	0.178	0.121	0.074	0.043	0.018
STREHL RATIO	0.13	0.34	0.49	0.66	0.79	0.91

Table 1: Coronagraph on-axis throughput for the base line 170 nm RMS wavefront error NGAO system configuration (see table 3), and the corresponding Strelh Ratios.

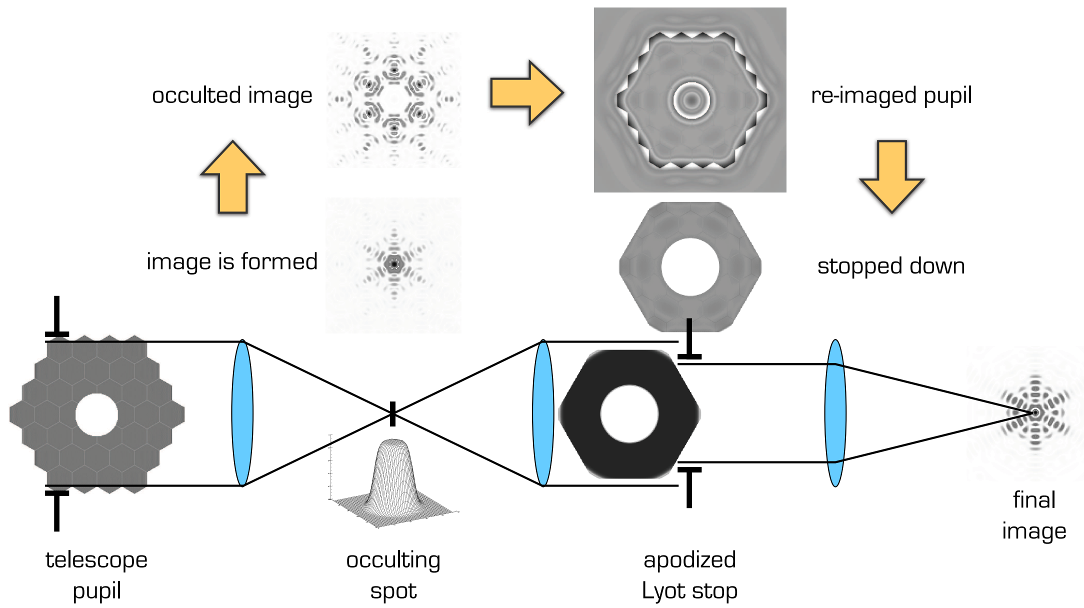

Figure 3: Schematic of a simple apodized Lyot coronagraph used for the numerical Monte Carlo type simulations of the NGAO configuration. The occulting spot size was varied between 6–14 λ/D for wavelengths between 0.7–3.5 μm.

3 Analysis methods

For the purpose of a contrast-oriented performance budget it is required to estimate the contribution to the local PSF contrast from the various sources of wavefront error that also feature in the general wavefront error budget (cf. KAON 471). Requiring that this also be evaluated as a function of the PSF image plane coordinate, amounts to a rather tall order. Among the standard analysis tools for AO that might be applied to this task we have:

1. Simple parametric models of the AO PSF (e.g. core+halo models). As mentioned already, core+halo models address only the global PSF morphology, and do not realistically model small-scale brightness variations.

2. Analytical models based on PSF calculations in spatial frequency domain. This method allows the modeling of PSDs from individual error sources as desired for the performance budget, from which PSFs and contrast values can be computed. This is often useful and can be highly accurate for some specific error terms, but can become intractable for other terms that have no simple analytical form in this Fourier domain modeling. Another catch is that it computes infinite long-exposure PSFs, meaning that atmospheric speckles are completely averaged out in the result. Since residual speckles are one of the most important sources for contrast degradation, the effect of finite-exposure speckles must here be modeled by some external means that adjusts the contrast estimation.

3. Numerical end-to-end AO simulations of the Monte Carlo (random phase screen) type can produce a very complex and realistic AO PSF from which the contrast can be computed directly by using the formula (1) – but they make it very hard to separate individual terms. Such simulations offer the highest level of sophistication but are often impractical as optimization tools if the parameter space is not already well constrained, and disentangling the contributions from different error sources can be either very hard or prohibitively time-consuming.

4. One may consider combining number 2 in this list with a reverse-engineered 3, i.e. trying to extract or estimate PSDs of individual terms from numerically simulated PSFs, and insert those as models in the analytical frequency domain computation (e.g. simply as a power law).

The analysis presented in this report is based on studies conducted using two separate computational tools, which employ, respectively, the methods 2 and 3 above. Method 4 was also used as an experiment for one single component of the PSD (the tomography error, see Sect. A.2.4). The use of multiple methods are rationalized as we must accept that neither is all-inclusive, but that they complement each other in different areas.

The analytical contrast calculation tool based on the method 2 above (a spread sheet calculation, henceforth referred to simply as the "contrast tool," or the "analytical tool") fills the function of producing a contrast-driven performance budget with separable error sources and the ability to easily trace the impact of individual terms on the overall performance. This calculation is parameterized and fast, but its realism is limited and it does not model certain error sources very realistically at all (see below). Therefore it is very useful to explore parametric behavior and for getting answers quickly, but its results should not be trusted as accurate to more than roughly one order of magnitude. To get more accurate results, detailed numerical simulations of a much more cumbersome nature are required, and that is where the second simulation tool comes in, providing just that.

The numerical AO simulation tool used for the current simulation results was the freely available Yorick Adaptive Optics (YAO) package (with some in-house Keck-specific additions and a new coronagraph module). Although the application of YAO to high-order AO systems is somewhat limited in scope by its simplistic wavefront reconstruction algorithm, the current high-contrast NGAO configuration (as detailed further in Sect. 4.3) was still at the level where the tomographic reconstructor was able to deliver acceptable performance. Some residual waffle patterns may be observed at a low level, but they are not a significant source of wavefront error. Anticipating some of the results to be presented, configured as a 5-LGS narrow-field quincunx AO system of order 36×36 (sub-apertures across the base of the Shack-Hartmann sensor), the NGAO setup was able to deliver down to 160 nm RMS residual wavefront error under typical conditions, all-inclusive. As already mentioned, the two tools complement each other in different areas of sophistication, realism and speed. Here is a (partial) list of wavefront error sources that are modeled by each tool and their degree of realism.

- The analytical contrast tool models the following errors well (+), tolerably (∼), and not at all (—):
  - \+ Fitting error
  - \+ Spatial aliasing
  - \+ Servo-lag
  - \+ Noise
  - \+ Tip/tilt errors
  - ∼ Tomography (power law approximation)
  - ∼ Quasi-static LGS errors (power law approximation)
  - ∼ Telescope static errors (power law approximation)
  - ∼ Instrument static errors (residual calibration errors)
  - — No detailed coronagraph model
  - — No detailed telescope aperture diffraction model
- In addition to the first five items listed above as being well modeled by the contrast tool, the numerical simulations also models the following effects with high fidelity (+) and some others not at all (—):
  - \+ Segment gaps (grey pixel approximation)
  - \+ Segment static aberrations
  - \+ Segment vibrations
  - \+ Telescope wind-shake (common-path)
  - \+ Tomography and LGS
  - \+ Coronagraph effects
  - — No instrument aberration calibration errors
  - — No optical quality residual aberrations

Only a few brief comments on some of the entries in this list, leaving some additional modeling details for Sect. A. Obviously the segmentation of the primary mirror is a major source for speckles and local brightness variations that complicate things like planet detection, and which needs to be addressed in detail by any study that cares about the PSF. The contrast tool currently has no specific diffraction modeling. Instead, a number of important segment effects are included in the numerical simulation code. Telescope static errors (segment figures, etc) are currently modeled in a generic way by the contrast tool (approximate PSD), but can be (and is) modeled with realism (segment figures measured with UFS, see KAON 468) by the numerical simulation code.

Wavelength Band	central λ (μm)	FWHM (μm)	color correction	zero point flux (10^{10} photons/s)	sky brightness (mag/arcs^2)
U	0.366	0.052	-0.2	19.6	20.90
B	0.438	0.100	-0.6	68.4	22.13
V	0.545	0.083	0.0	40.6	21.99
R	0.641	0.157	0.6	54.1	20.81
I	0.798	0.154	1.3	34.2	20.25
J	1.22	0.260	2.7	26.3	19.60
H	1.63	0.290	3.8	14.2	17.09
K$'$	2.12	0.410	4.9	9.39	16.99
K	2.19	0.320	4.8	8.02	16.78
L	3.45	0.570	6.8	3.67	9.91

Table 2: Photometric system used for simulated observing scenarios. Based on the Johnson-Cousins-Glass system from Bessel et al. (1998), as outlined in the NGAO_Perf_Budget_Template.xls document (available at the NGAO Twiki site). The zero point was computed for a collecting area of 79 m^2, and is the photon flux at the Keck Nasmyth from a $V = 0$ star.

4 Contrast estimation

This section employs the analytical and numerical tools to produce contrast and wavefront error budgets for the base line NGAO configuration, and examine some details that influence the performance. A closer analysis and discussion of how well the base line NGAO configuration is able to meet the science requirements are deferred to Sect. 5.

4.1 System and atmosphere assumptions

The starting point for the NGAO configuration implemented in the contrast tool was the 155 nm "Exo Jup LGS" (at zenith) wavefront error budget presented in Appendix 2 of KAON 461, adjusted here to $N = 36$ sub-apertures across the pupil, and other wavefront error (WFE) terms modified to produce a total of 170 nm RMS (including tip/tilt) in accordance with the numerical simulations. The resulting wavefront error budget is shown in Fig. 4. The numerical simulation also produces a total wavefront error of 170 nm RMS, but care must be exercised in comparing to the WFE budget in Fig. 4. The simulation WFE pertains to the AO system performance, while the WFE budget of the contrast tool reports performance at the image plane of the science instrument. Hence the final table in Fig. 4 includes some instrument calibration errors not present in the numerical simulation, and it does not include tip/tilt error. Accounting for these two differences produces consistent results between the modeling methods, with a total AO WFE of 170 nm and the high-order part (in quadrature) at 164 nm.

Parameter	Contrast tool	YAO numerical simulation
Telescope diameter	$D = 10$ (circular)	Keck segmented pupil (grey pixel approximation)
Turbulence parameters	$r_0 = 0.18$, $\bar{v} = 8$ m/s	CN-M3 7-layer turbulence model
WFS sub-apertures	36×36	36×36 (determines fitting and aliasing in both methods)
WFS measurement error	input: 80 nm	intrinsic: $m_{589} = 9$, spot elongation, fratricide
Servo-lag error	input: 40 nm	intrinsic: 1 kHz frame rate, integrator
Tomography error	input: 76 nm	intrinsic: 5 Na-LGS at 90 km in 11$''$ quincunx asterism
Tip/Tilt error	input: 40 nm	intrinsic: 3 NGS (J=16) in 30$''$ triangular asterism
Static instrument errors	30/30 nm (low/mid)	—
Static telescope errors	input: 70 nm	static segment figures: 65 nm residual error
LGS quasi-static errors	input: 60 nm	— (not sure what this includes)
Exposure time	$\tau_e = 10 - 1800$ sec	$\tau_e = 30$ sec (lower limit on speckle noise from simulation)

Table 3: Base line NGAO system configuration, highlighting the areas where the analytical contrast tool and the numerical simulation tool differ in their assumptions and implementation. "Intrinsic" implies that a quantity in the numerical simulation is included but is an emergent property, depending on other parameters, while "input" for the contrast tool means that a value must be entered, which is then used to scale a corresponding PSD model for that error term.

AO, telescope, atmosphere			
D	**10**	meters	primary mirror diameters
N	**37**		Number of actuators across 10-m primary
r0	**0.18**	m	at 500 nm
Strehl from tilt/LOWFS	**0.95**		
wind velocity	**8**	m/s	used for specke lifetimes
AO frame rate	**1000**	Hz	used for speckle lifetimes

Science parameters						
λ_sci	**1.25**	microns	science waveleng	8	0.025783828	lambda/D
θ	**0.2062706**	arcseconds	angle of interest		5.29E-04	contrast
Science zeropoint	**27.5**	magnitudes	magnitude of star producing 1 photoelectron/second on detector			
Science bandwidth	**0.25**	microns	used primarily for speckle elongation			
Integration time	**30**	seconds				
Target magnitude	**15**	magnitudes	at science wavelength			
SSDI speckle suppression	**1**	reduction in speckle noise due to post-processing.				

Dynamic WFEs			
WFS meas.	**80**	nm	
Servo lag	**40**	nm	
Tomography	**75**	nm	
Static WFEs:			
Initial science-path error	**150**	nm	total at all frequencies
Low-freq. Calibration	**30**	nm	Residual after image sharpening calibration
Mid-freq. Calibration	**30**	nm	Residual after image sharpening calibration
LGS quasi-static errors	**60**	nm	Finite spot size, etc.
Telescope static errors	**70**	nm	After AO correction

Speckle lifetimes		
Atmosphere speckles	0.75	seconds
AO control speckles	0.01	seconds
Static speckles	**600**	seconds

	Low freq.	Mid. Freq.	High Freq.		Total WFE
Frequencies	4	(...)	18.5	cycles/pupil	nm
	0.4	(...)	1.85	cycles/meter	
Atmosphere fitting error			61.2	nm	61.2
Aliasing error		33.5		nm	33.5
WFS measurement		80.0		nm	80.0
Servo lag		40.0		nm	40.0
Tomography		75.0		nm	75.0
Calibration and static errors	30.0	30.0	3.6	nm	42.6
LGS quasi-static errors		60.0		nm	60.0
Telescope		70.0		nm	70.0
Total high-order WFE					169.7
Total strehl					0.5

Figure 4: Base line NGAO configuration and wavefront error budget for the 165 nm RMS (counting only high-order errors) "Exo-Jupiter" science case. The corresponding contrast budget is shown in Fig. 5. Atmospheric parameters and the dynamic WFS errors that depend on them were adopted from the CN-M3 turbulence model with $r_0 = 18$ cm (see KAON 303). Photometric zero points and bandwidths used values from the photometric system defined in table 2. Additional 45 nm and 42.6 nm RMS arise from the assumptions on residual low-order tip/tilt error (J band Strehl $S = 0.95$) and residual instrument calibration errors. The values of input wavefront error parameters were adjusted to be consistent with and as close as possible to values counted in a much more detailed wavefront error budget obtained with the WFE spread sheet tool (KAON 471), which are also consistent with the numerical simulation results. Fields in blue are the parameters that are varied from this base line configuration to explore their impact on the contrast.

	Speckle time (sec)	PSF intensity Normalized peak=1	Photon noise	Long-exposure speckle noise	Post-SSDI speckle noise	SSDI factor
Atmosphere fitting error	0.75	1.8E-11	7.70E-09	2.9E-12	2.9E-12	1
Aliasing error	0.75	5.4E-05	1.34E-05	8.6E-06	8.6E-06	1
WFS measurement	0.01	3.3E-04	3.30E-05	6.1E-06	6.1E-06	1
Servo lag	0.75	7.3E-05	1.55E-05	1.2E-05	1.2E-05	1
Tomography	0.75	1.7E-04	2.37E-05	2.7E-05	2.7E-05	1
Calibration and static errors	600	4.0E-05	1.15E-05	4.0E-05	4.0E-05	1
LGS quasi-static errors	600	1.8E-04	2.41E-05	1.8E-04	1.8E-04	1
Telescope	600	2.6E-04	2.90E-05	2.6E-04	2.6E-04	1
Total		1.1E-03	6.02E-05	5.3E-04	5.3E-04	
Total speckle+photon final contrast					5.29E-04	

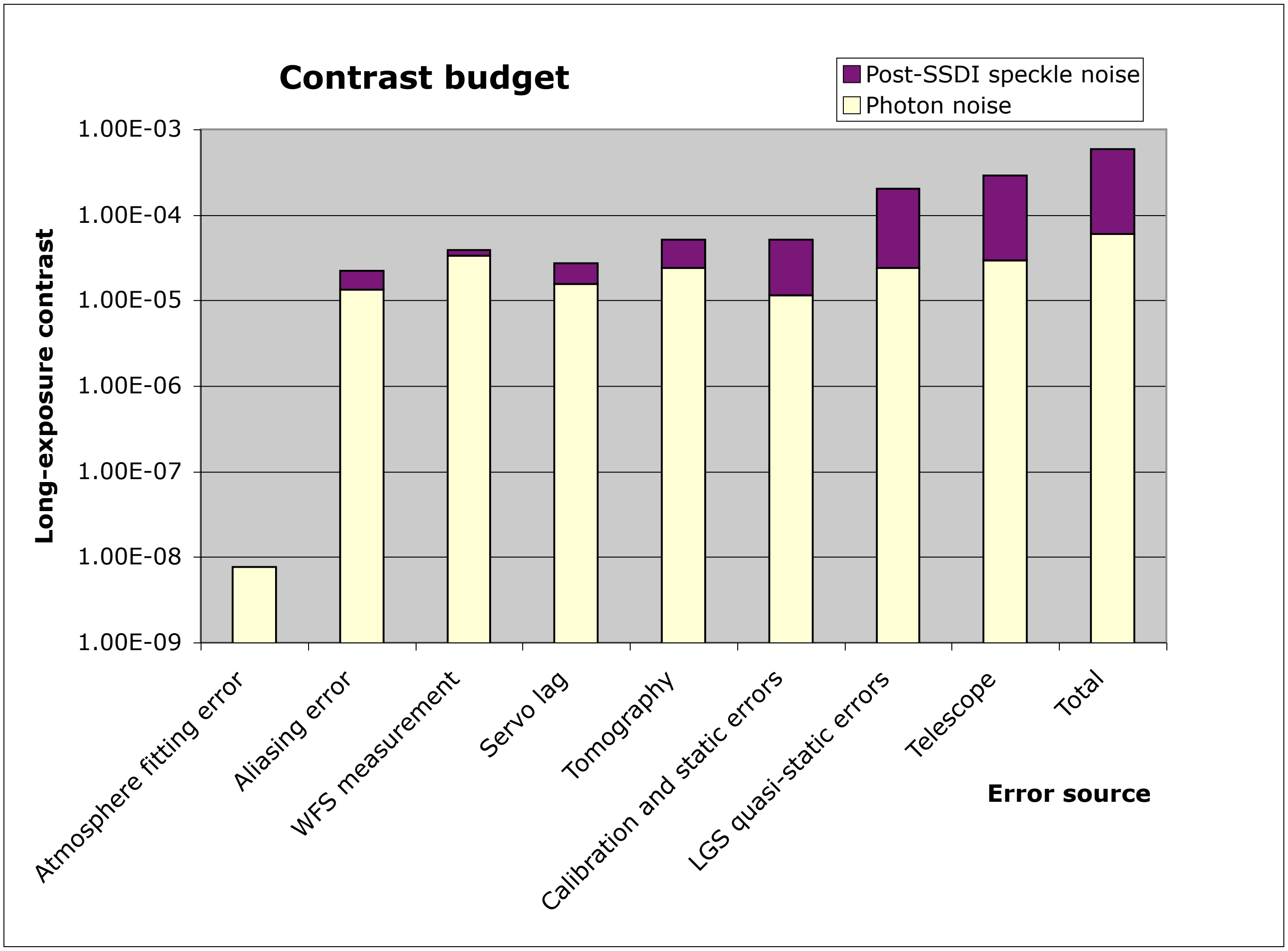

Figure 5: Sample J-band (1.25 μm) contrast budget evaluated at 0.2 arc seconds, for the baseline NGAO configuration (Exo-Jupiter scenario) and 165 wavefront error budget as outlined in Fig. 4.

The simulation uses the 7-layer CN-M3 turbulence model from KAON 303, with $r_0 = 0.18$ m, $\theta_0 = 2.5''$, $\tau_0 = 3.4$ ms and $d_0 = 4.4$ m. The only atmospheric assumptions explicitly going into the contrast tool are the overall seeing and the average wind speed $\bar{v}$, which are set to $r_0 = 0.18$ cm and $\bar{v} = 8$ m/s respectively. For instance, the influence of the turbulence profile on the tomography error in the contrast tool has to be accounted for within the value of that term, which was read off from the ExoJup LGS budget summary to be 76 nm. In comparison, The YAO simulation uses 5 LGS in a narrow-field ($11''$ radius) quincunx asterism and three tip/tilt NGS within a $1'$ field for focus and astigmatism compensation, whereby the tomography error is an intrinsic and emergent property of the AO system configured this way.

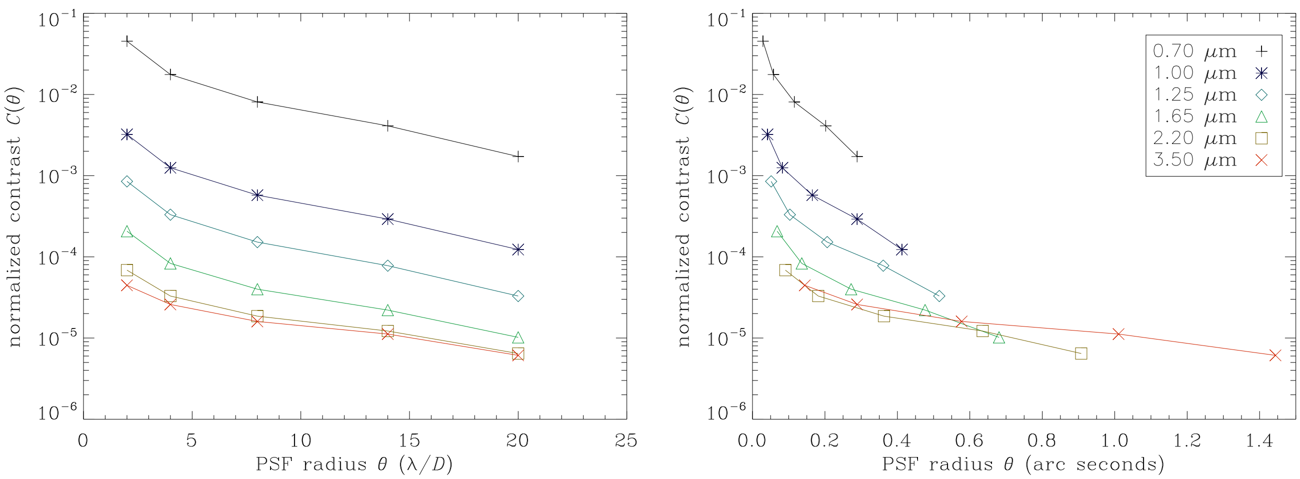

Figure 6: Contrast versus wavelength and PSF radius for the 165 nm Exo-Jupiter NGAO configuration in Fig. 4, plotted both versus units of λ/D (left) and in arc seconds (right) for clarity. The evaluations points were at 2, 4, 8, 14 and 20 λ/D.

4.2 Analytical contrast tool

Starting with the analytical contrast tool, we need to note a few caveats. Since it does not have a detailed diffraction or coronagraph model, contrast values obtained inside of $\sim 5\lambda/D$ should be read with caution, deferring analysis of coronagraph performance until the numerical simulations are interrogated. In the other direction, the tool is currently unable to perform calculations outside of AO working range, as defined by the angular cut-off frequency α_c of the AO system (a future version of the tool will remove this limitation). This parameter in turn is governed by the AO inter-actuator distance d and the imaging wavelength λ according to $\alpha_c = \lambda f_c$, where f_c is the AO spatial cut-off frequency $f_c = 1/2d$. Expressed in units of λ/D the angular AO cut-off frequency is $\alpha_c = N/2$, where N is the number of sub-apertures across a pupil of diameter D, assuming that $Nd = D$ (it is also assumed here that actuator pitch and sub-aperture size are the same). For the base line NGAO system assumed in this study ($N = 36$) on the Keck telescope ($D = 10$) we find that $f_c = 1.8$ m^{-1}, and $\alpha_c = 18\lambda/D$. This is the outer limit for evaluating the contrast using this spread sheet tool.

Since the PSDs of the analytical contrast tool can not account for noise and speckles in the science image (while it does include noise effects in the WFS) by nature of the infinite exposure time assumption, these two effects have to be modeled separately. The contrast tool does this by defining the total contrast as the quadratic mean of photon and speckle noise terms separately:

$$C(\theta) = \sqrt{\sigma_n^2(\theta) + \sigma_s^2(\theta)}, \tag{2}$$

where σ_n^2 and σ_s^2 are the mean-square brightness variations due to photon noise and speckle noise respectively, computed over the aperture $\mathcal{A}$ in the PSF and azimuthally averaged. The sigmas in turn are modeled as:

$$\sigma_n^2(\theta) = (\eta N)^{-1}\sqrt{\langle K(\theta)\rangle_{\mathcal{A}}}, \tag{3}$$

$$\sigma_s^2(\theta) = C_0(\theta)\frac{\sqrt{\langle K^2(\theta)\rangle_{\mathcal{A}}}}{\langle K(\theta)\rangle_{\mathcal{A}}}\left(\frac{\tau_s}{\tau_e}\right)^{1/2} \tag{4}$$

where η is the throughput, N is the total number of science photons of the exposure, and τ_e and τ_s are the exposure time and speckle life time. The aperture $\mathcal{A}$ should be on the order of a few λ/D, reflecting the assumptions on the extension of the observed object. If point-like, use $\mathcal{A} = 2\lambda/D$. The formulas (2)-(4) are used in the analytical companion sensitivity spread sheet tool. Note that the standard core-halo contrast $C_0(\theta)$ appeared as one element in σ_s^2. The default science observing scenario assumed a science integration time of 1800 seconds (30 minutes) and a default speckle suppression factor of SSDI=2, with other parameters as given in Fig. 4 and table 2.

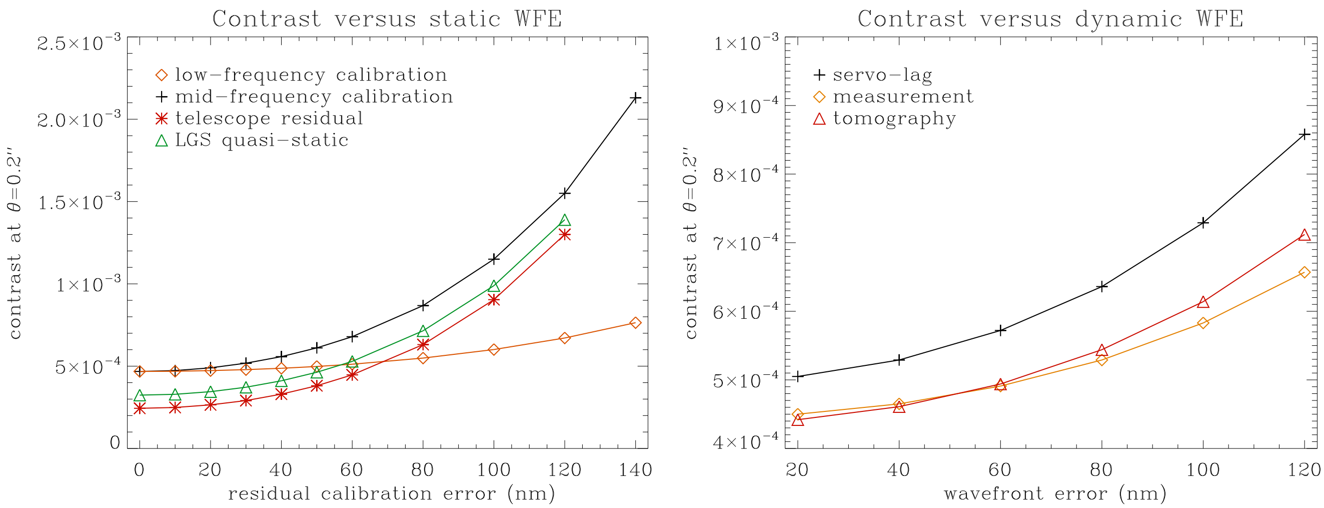

Figure 7: Static and dynamic wavefront errors in the J-band base line NGAO configuration, evaluated at 0.2″.

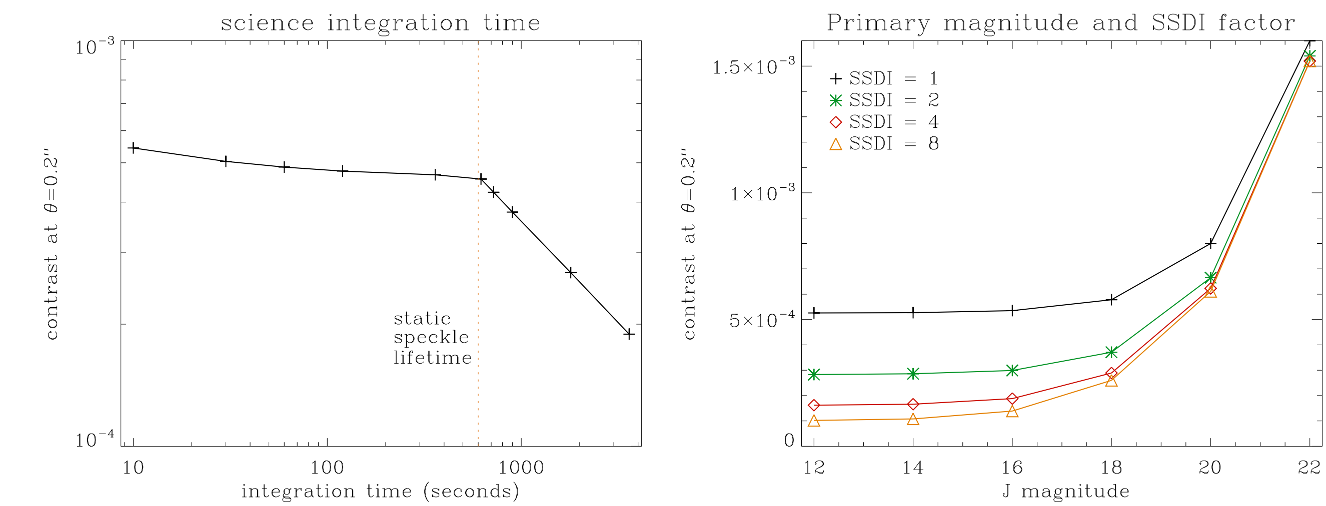

Figure 8: The effects of science integration time and post-processing speckle suppression (SSDI factor) in the J-band base line NGAO configuration, evaluated at 0.2″.

4.2.1 Sample numerical results

A sample J-band contrast budget evaluated at 0.2″ corresponding to the NGAO configuration and wavefront error budget in Fig 4 is shown in Fig. 5. This sample case was evaluated for a 30 second exposure, for comparison with the numerical simulation, and therefore also with no additional speckle suppression (SSDI=1). The plots of contrast versus wavelength and PSF radius shown in Fig. 6 used the default science observing parameters instead, with a total exposure time of 30 minutes and a modest speckle suppression factor SSDI=2. There is no sky background present in these contrast estimations, which would mainly affect the L-band contrast (and to a small extent K band) and contrast in the outer region of the PSF halo if included. Figures 7 and 8 examines the influence of varying one parameter at the time, all other parameters keeping their nominal values. What is reported is the change in the *total* contrast as a function of a given parameter.

Figure 7 shows the scaling laws of static and dynamic wavefront errors on the contrast. On the left, residual static aberrations in the middle-frequency range are seen to be the most harmful. This is consistent with the observation that high-frequency aberrations tend to scatter light further out into the halo, and that both high- and low-frequency residuals will appear more or less smooth on the scale of the integration aperture $\mathcal{A}$. Telescope residual and LGS

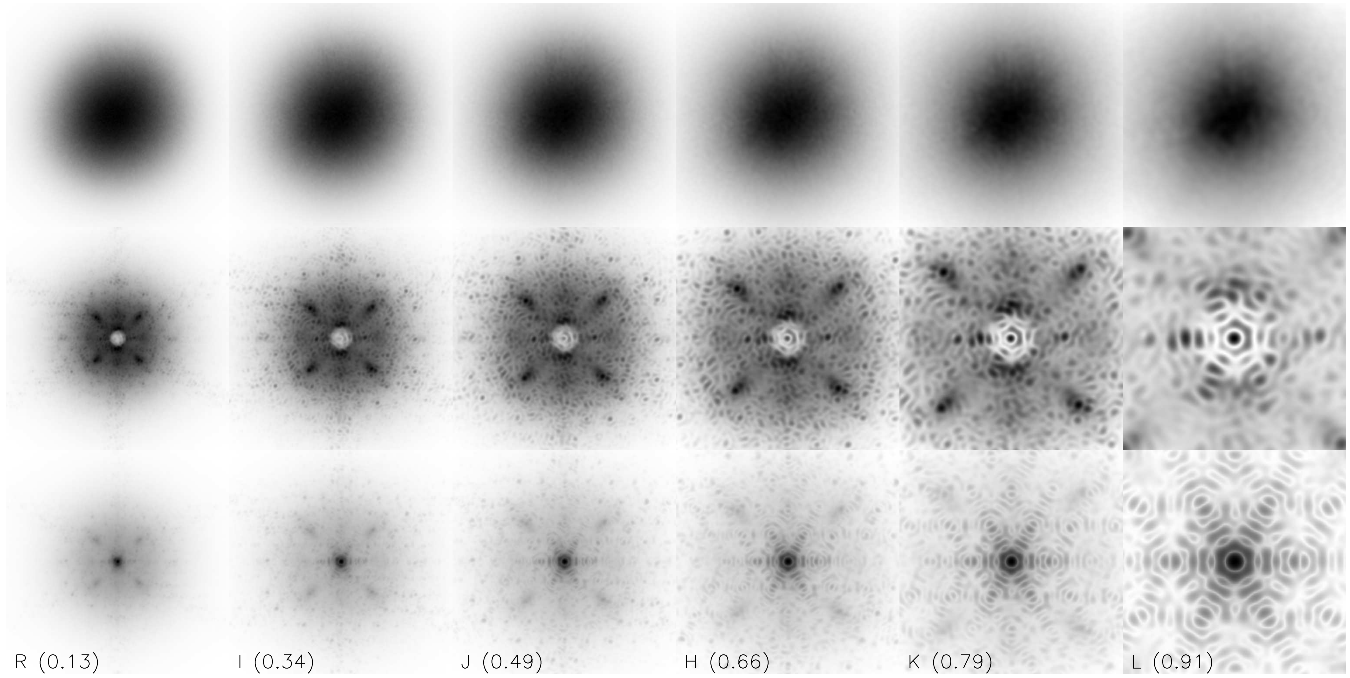

Figure 9: PSFs from 30-second NGAO simulations, ranging from R to L band and showing the AO PSF (bottom row), the on-axis coronagraph image (middle row, $10\lambda/D$ occulting spot, no companion inserted), and the seeing-limited image (top row). The field of view of each image is 1.8 arc seconds. All images are stretched (asinh) and individually byte-scaled.

quasi-static errors show the same scaling as the mid-frequency instrument calibration error, but on a per-unit-residual basis their impact on the contrast is far less. On the right, the three kinds of dynamic wavefront error are seen to follow roughly the same scaling laws, but the shape of the servo-lag PSD is seen to make it the most harmful component to the contrast. This is consistent with other high-contrast studies for planet finding instruments (e.g. SPHERE, GPI) that all conclude the necessity to run the AO system at high frame rates to greatly reduce servo-lag. **[ref. for this?]**

Figure 8 investigates the character of the contrast tool calculation as a function of science exposure time and the application of speckle mitigation strategies. On the left, the modeling of what happens at the break point of the static speckle life time may appear a bit unphysical, but the details of this would only matter if you are interested in the behavior close to this limit. In the current study, the contrast tool is only used at two widely separated points in parameter space: 1800s exposure for the science evaluation, and a 30s exposure for comparison with the numerical simulation, which are well above and below the threshold that the details around the break point are unimportant. On the right, we observe a transition in the contrast from speckle noise dominated to photon noise dominated as the brightness of the primary star decreases. The effect of post-processing speckle suppression is also seen to be reduced as photon noise takes over. In the speckle noise dominated regime, post-processing can potentially improve contrast by a significant factor. In the contrast tool, speckle suppression is modeled simply as a linear attenuation of the speckle noise sigma component.

4.3 Numerical AO simulations

Moving on to the numerical AO simulation, it is as stated in many ways a much more realistic representation of the AO system, but it does not directly allow the wavefront error to be broken down into a itemized budget, and consequently neither the contrast. Furthermore, by the demanding nature of the computations involved, no exposures longer than 30 seconds have been generated for the study so far (30 seconds of simulated real time took 56 hours to render). Therefore a limited set of representative cases had to be selected for this study, and while PSFs were obtained for the whole wavelength range of interest, when proceeding to construct the simulated observations only the J band case has been examined in detail so far.

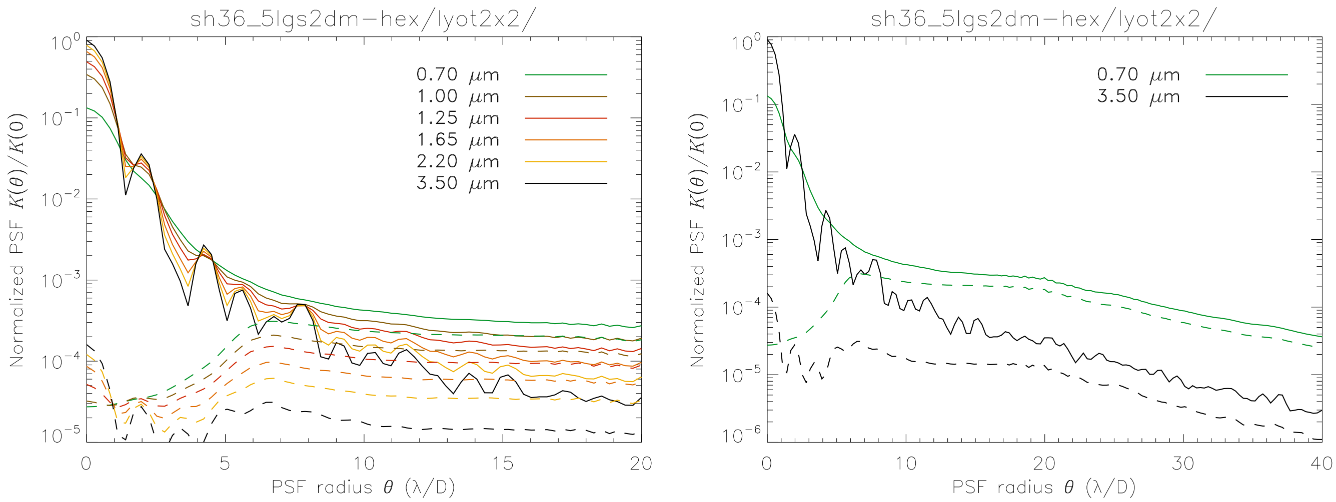

Figure 10: Normalized radial PSF profiles (azimuthally averaged) with (dashed lines) and without (solid lines) a $6\lambda/D$ coronagraph. Two different ranges and selections of curves are shown for clarity.

4.3.1 System configuration

The base line configuration was outlined in table 3. In a previous version of this report (03/18/2007), simplified AO configurations were employed for the purpose of interrogating the effects of e.g. segment vibrations and telescope wind shake isolated from all other effects. That analysis was omitted from the current version of the report, in favor of emphasizing the all-inclusive NGAO simulations carried out since. In addition to static segment figure errors, a low (but realistic) level of wind shake and 30-Hz segment vibrations were also included in the current simulations. Their power spectra (as modeled) are shown in Fig. 14, and it is including these disturbances that the total wavefront error of the base line NGAO configuration simulated here amounts to 170 NM RMS. It was indicated in the previous study, however, that wind-shake-induced common-path aberrations have a very mild and even negligible effect on the contrast, since the errors are all tilts (i.e. low-frequency). Segment vibrations on the other hand seemed to potentially have a more severe impact on contrast, being stronger in the middle frequencies. Recent observations however suggest that the actual power in segment vibrations may be closer to the lower end of the range previously allowed for [ref. Cneyman]. So segment vibrations are included, but their residual is a small part of the AO simulation wavefront error.

4.3.2 Numerical results

An example of the output from a YAO AO simulation with a coronagraph is shown n Fig. 9. Normalized radial profiles of the AO PSF and AO+coronagraph images are shown in Fig. 10. It is seen that, on the whole, a generic type of apodized Lyot coronagraph is doing a fair job of blocking the light from the primary star and reducing the amount of scattered light. These results characterize the AO performance, but before proceeding to compute contrast numbers it is necessary to specify an observing scenario.

4.3.3 Simulated observation

We are interested in emulating a long exposure, on the order of ∼30 minutes, as is foreseen to be required for beating down various noise sources in order to detect a faint planet in the halo of a nearby star. Unfortunately the speckle characteristics of the AO simulation are frozen at 30 seconds. It was opted to not try and do anything clever about this, but simply use that as-is. This means that the end result will be pessimistic with regards to overestimating the speckle noise, but optimistic with regards to not including any residual and un-calibrated instrument aberrations. Since we are aware of this, we will be able to interpret the results accordingly. To simulate electronic and photon noise on the image frames, the observation was modeled as 60 separate 30-second exposures, and a host star magnitude needs to be assumed, with sky backgrounds and zero points as in table 2. This observation was to be in J band,

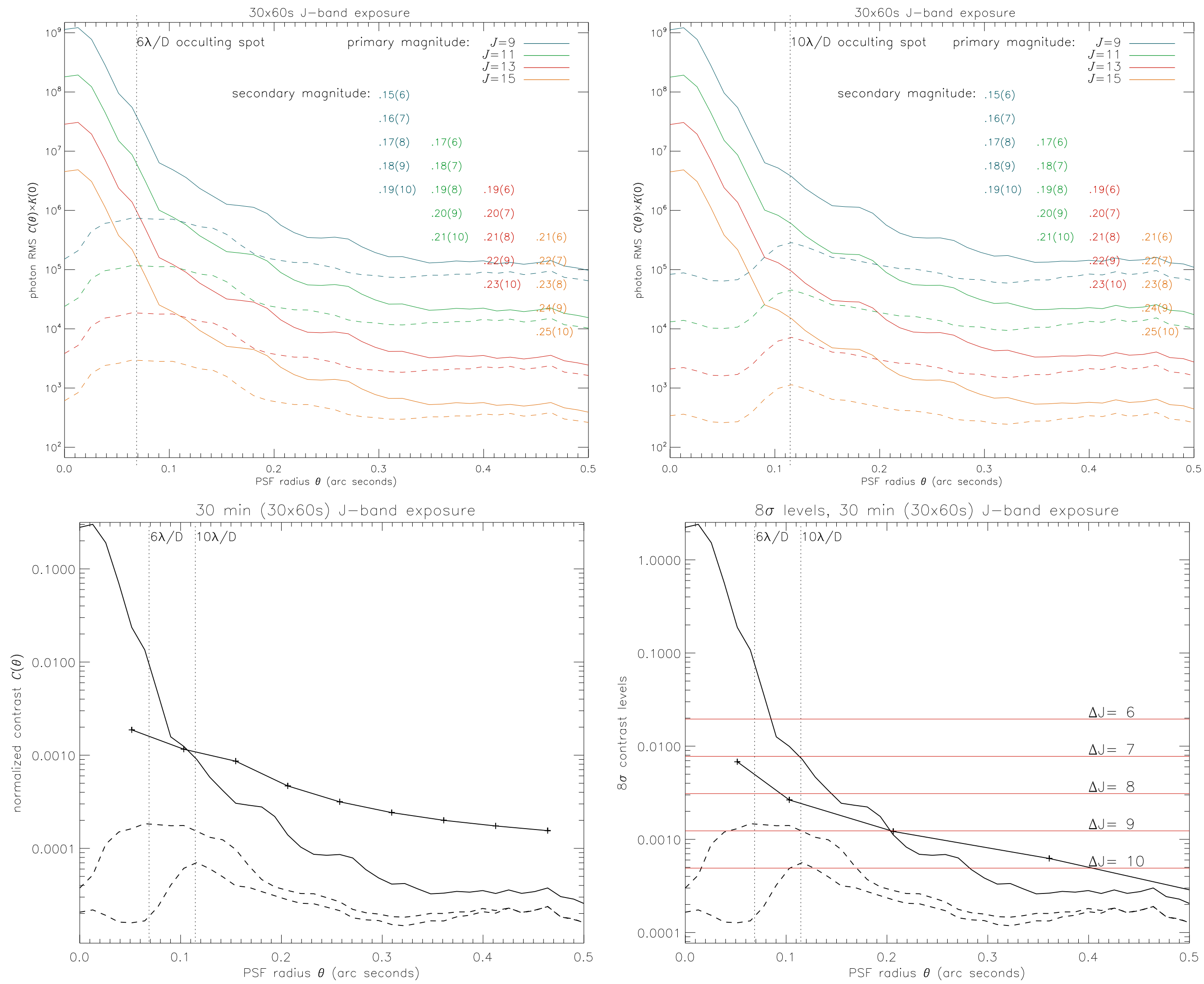

Figure 11: Photon-scaled standard deviations (top row) and normalized contrast $C(\theta)$ (bottom row) for the clear AO (solid curves) and coronagraph (dashed lines) cases at $6\lambda/D$ (top left) and $10\lambda/D$ (top right) occultations.

with primary magnitudes between J=9-15. The detector specifics were set to 2.5 e^- RMS/pixel read-out noise, 0.01 e^-/pixel/sec dark current (generic HgCdTe NIR array), pixel sizes roughly $\sim \lambda/(2D)$, and a total transmission from the Keck Nasmyth to the detector (including QE) of 0.5. It was assumed that there is a differential rotation between the AO system and the sky, so that the science targets stay fixed on the science detector while the pattern of the PSF rotates at the sidereal rate.

The normalized contrast $C(\theta)$ can be then computed on the resulting images for a quantitative analysis and comparison with the corresponding predictions by the analytical contrast tool, as shown in Fig 11. There is some redundancy in this figure, as some graphs were split into two for clarity. The top two panels show the photon-scaled standard deviations (i.e. the contrast un-normalized) of the four science scenarios with primary magnitudes $J_1 = [9, 11, 13, 15]$, with the corresponding photon levels of a range of delta-magnitudes $\Delta J = 6 - 10$ superimposed for each case. These levels of the secondaries were calculated by integrating the AO PSF over the same aperture $\mathcal{A} = 2\lambda/D$ as used for the contrast calculation, assuming the same spectral type and wavelength as the primary (an invalid but necessary assumption at this time). Accepting the embarrassing fact that photon noise made absolutely no difference to the relative contrast between the observing scenarios in this regime of the PSF (and here I went to all the trouble), the four curves of different primary magnitudes in the top two graphs can be compressed into one

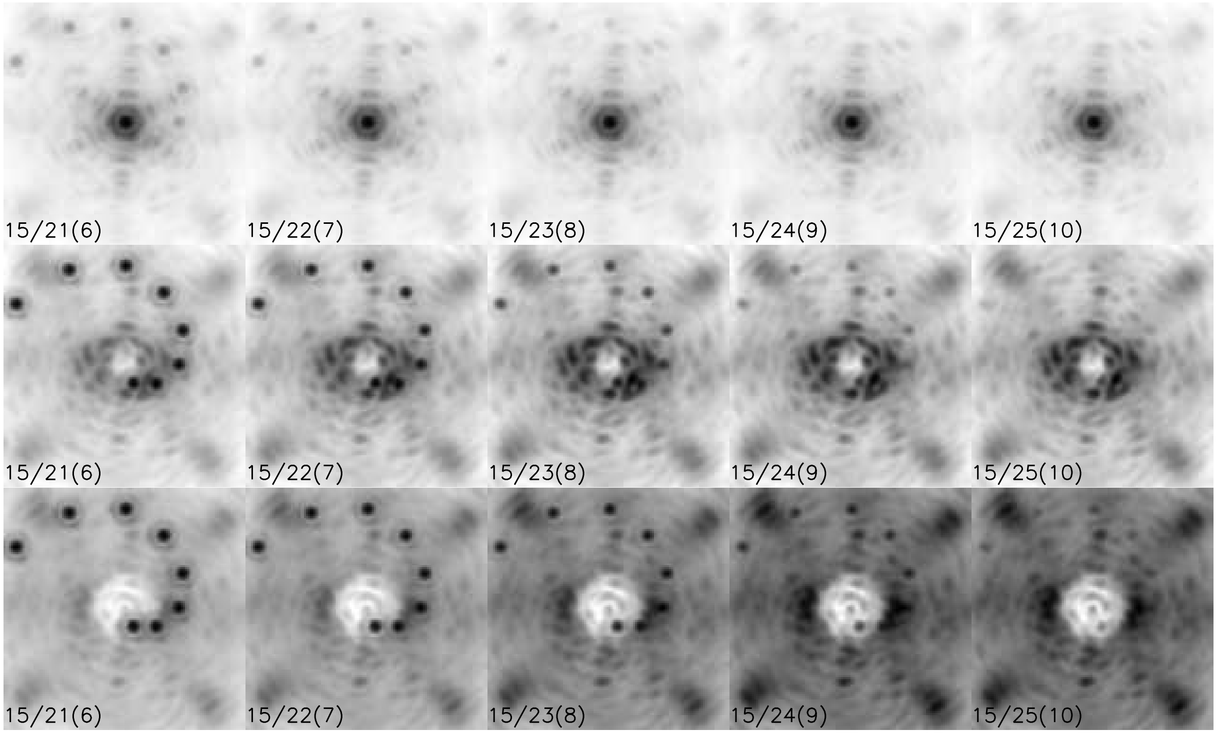

Figure 12: Simulated J-band science observation with secondary objects inserted. Top row: AO without coronagraph; middle row: AO+coronagraph with $6\lambda/D$ occultation; bottom row: AO+coronagraph with $10\lambda/D$ occultation. The numbers in the lower left corner of each image indicate the primary/secondary/delta magnitudes, i.e. the format is $J_1/J_2(\Delta J)$. The images are stretched (asinh) and individually scaled.

and normalized to yield the contrast $C(\theta)$, which is what is shown in the bottom two graphs of Fig. 11. These two graphs warrant further discussion, which is postponed to Sect. 5.

In addition to calculating contrasts, while a lot of fun in itself, it can also be elucidating to see what it would actually look like if there were secondary companion objects in the halo of these primary stars. Hence the second stage of the simulated observation injected a series of weaker point sources in a spiral around the primary, and recomputed the noise and rotation etc. A representative cut of these images are shown in Fig. 12, where only the $J = 15$ case is shown for $\Delta J = 6 - 10$. The first 8 companions that are within the field of view are positioned at radii of 6–34 λ/D in increments of 4. This means that the first one would be blocked by the coronagraph with a $10\lambda/D$ occulting spot. The next stage of the analysis would involve an attempt of PSF subtraction in order to assess the ability to detect the companion sources, but in order to be fair this requires an entirely separate model or estimation for the PSF to be subtracted, which is work that has not been carried out yet.

5 Evaluation and Conclusions

This section will focus on the two graphs in Fig. 11 in the lower right and lower left panels, and also referring to Fig. 13. Starting with the lower left, this figure shows the normalized contrast of the 30-minute J-band simulated observation, where we recall that the speckle noise has the characteristics of only 30 seconds exposure (excepts for the slight rotation of the PSF that blurs things out somewhat, however marginally). Over-plotted for comparison (solid line with pluses "+") is the prediction offered by the analytical contrast tool for the same scenario (i.e. no instrument WFE, no SSDI, and 30 second exposure time). The contrast tool makes a significantly more pessimistic prediction in this case. The question of whether a detection is enabled at a certain radial distance θ requires in addition to the contrast number a confidence level above which we are willing to declare a positive detection. A threshold of 8σ has been suggested as a relatively conservative level, where positive detections are still possible at a lower level but with an increased population of false positives. In the graph at the lower right of Fig. 11, the contrast

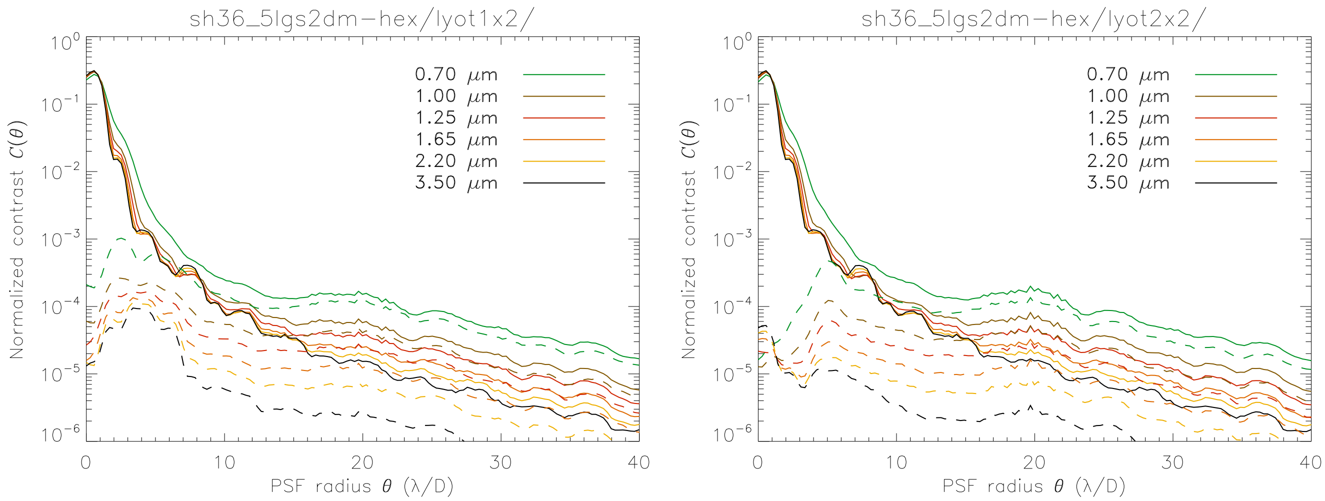

Figure 13: Normalized contrasts for the 30-second numerical simulation.

curves have been multiplied by 8 and the delta-magnitude levels are over-plotted in red, so as to make it easy to judge where the different cases clear the 8σ threshold (and where they do not). A prediction from the contrast tool is inserted again, but this time it is adjusted to 30 minute exposure time and with speckle suppression set to SSDI=2 (and the 30+30 nm residual calibration errors were switched on again).

At this point we recall the science goals introduced in Sect. 2.2. Reading off the chart at the lower right panel of Fig. 11, science goals 1 and 2b would be achieved in this simulated observation, by the 10 and 6 λ/D coronagraphs respectively, however fail without the use of a coronagraph. Goals 2a and 3 do not look likely to be achieved in this scenario by any stretch of the imagination – substantial improvements to the coronagraph design and control of static speckles (high-fidelity PSF subtraction) would appear to be required in order to achieve these goals. Science goals 4 and 5 can not be instructed by the J-band simulation of Fig. 11, but an estimate may be obtained from inspection of figures 6 and 13. By a simplified calculation, bypassing the rigor of producing noisy and rotated long-exposure PSFs in I and H band, the science goals 4 ($\Delta H = 5.5$ at $0.5''$) and 5 ($\Delta I = 7.5$ at $0.75''$) translates approximately into the contrast requirements $C(0.5'') \leq 0.0035$ in H and $C(0.75'') \leq 0.00025$ in I at the 8σ confidence level. From inspection of Fig. 13, both science goals 4 and 5 are seen to be achieved by a margin without a coronagraph even at the 8σ confidence level ($0.5''$ is 16.5 λ/D in H; $0.75''$ is 40 λ/D in I).

In judging the degree of achievement of the science goals by the present data, it must of course be kept in mind what the limitations are and the specific conditions underlying the simulated data set. Nevertheless, here's a summary of the one-shot contrast results and their implication on AO derived requirements. The asteroid science goals ($\Delta H > 5.5$ at 0.5", $\Delta I > 7.5$ at 0.75") are achieved by a wide margin with the base line NGAO configuration, and could realistically also be achieved by a much more modest AO system. Hence the asteroid science cases do not appear to drive NGAO high-order requirements beyond the point design (see NGAO Proposal), but rather can relax a number of design points, such as laser power (tomography error). The close companion (coronagraph) science cases are partially achieved by the same NGAO configuration:

1. $\Delta J = 10$ at 0.2". Achieved at a 8σ confidence level by either 6 or 10 λ/D coronagraph. Not achieved without coronagraph
2. a) $\Delta J = 8.5$ at 0.1". Achieved at a 8σ confidence level by $6\lambda/D$ coronagraph
   b) $\Delta J = 11$ at 0.2".Not achieved at 8σ confidence level. Achieved at 5σ confidence level by either 6 or 10 λ/D coronagraph.
   c) $\Delta J = 11$ at 0.1". Not achieved (factor 10 missing for 8σ level).
3. $\Delta J = 9 - 13.5$ at 0.07". $\Delta J = 9$ could be possibly be achieved at 5σ level by the $6\lambda/D$ coronagraph but would be close to the occulting disk.

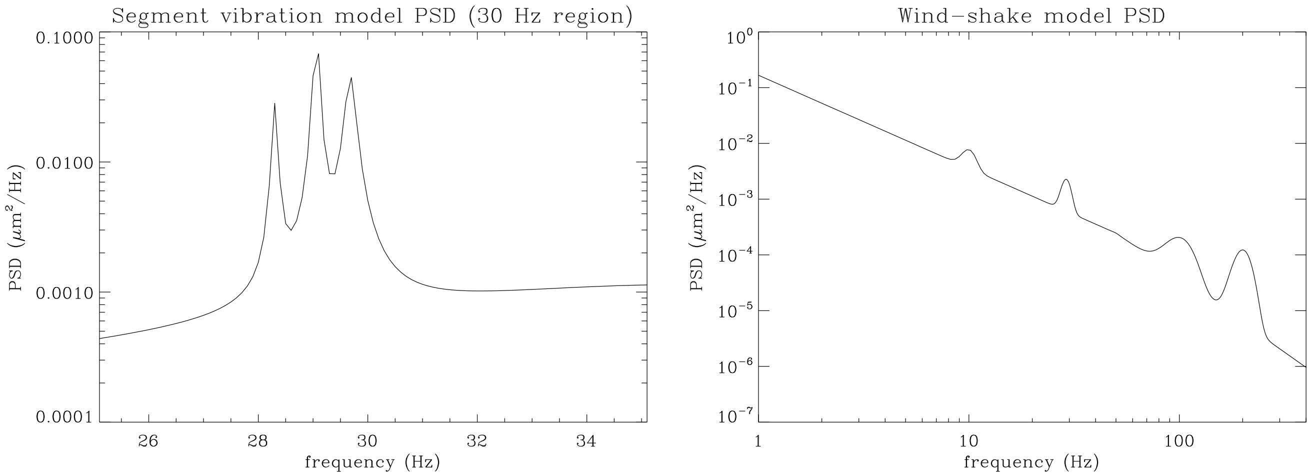

Figure 14: Temporal PSDs for the 30-Hz segment vibration model (left) and the wind-shake model (right) used in the numerical simulation code.

So in round numbers, 50% of the defined companion science cases appear to be achieved at a 6 to 8 σ confidence level by a standard coronagraph and the base line NGAO system configuration. The margins are much tighter here compared to the asteroid cases, but it is also recognized that speckle noise in this simulation is pessimistic and that good PSF subtraction and speckle suppression strategies may improve the current margins and bring some of the other goals within reach. That being said, the tall tent poles that must be controlled and minimized for these goals to stay achievable are 1) excellent calibration of static non-common path aberrations, 2) keep a high bandwidth $\geq$ 1kHz to minimize servo-lag, which has a strong impact on the contrast, and 3) effective application of speckle suppression techniques (whether by multi-channel differential imaging or highly precise PSF subtraction).

Appendix

A PSD modeling

This section offers some additional background material on various modeling aspects embedded into the analysis methods used in this report.

A.1 Temporal PSDs

Two model temporal power spectra were invoked in the numerical YAO simulation for the implementation of segment vibrations and wind shake, which are shown in Fig. 14. These models are based on combinations of sources (FSM measurements–Dekens thesis, JPL accelerometer data, see report by Erm). The segment vibrations were set to half the nominal value deduced by Dekens, amounting to an input RMS wavefront error over the whole pupil of 31 nm. Wind shake was added in at the level of 100 nm RMS, but since this was all in common path the tip/tilt subsystem of NGAO usually does a good job of compensating for most of it in this simulation.

A.2 Spatial PSDs

This section gives a brief overview of the analytical Fourier domain PSD models currently used in the contrast tool. While the tool currently uses open-loop formulas, some of the available closed-loop formulas are given below, with an encouragement for future revisions of the contrast tool to adopt the closed loop formulas. References for this section include [3, 2] and NGAO notes (available on Twiki – see Appendix B). Figure 15 shows a summary of the spatial frequency PSDs of the dynamic WFE terms that are modeled by the contrast tool, illustrating their various power laws. As a primer on the notation, the spatial PSDs are denoted by $\Phi(\mathbf{f})$, where $\mathbf{f}$ the the 2D spatial frequency vector. The models assume the Taylor hypothesis and a discrete layered C_n^2 profile divided into N_l layers, which

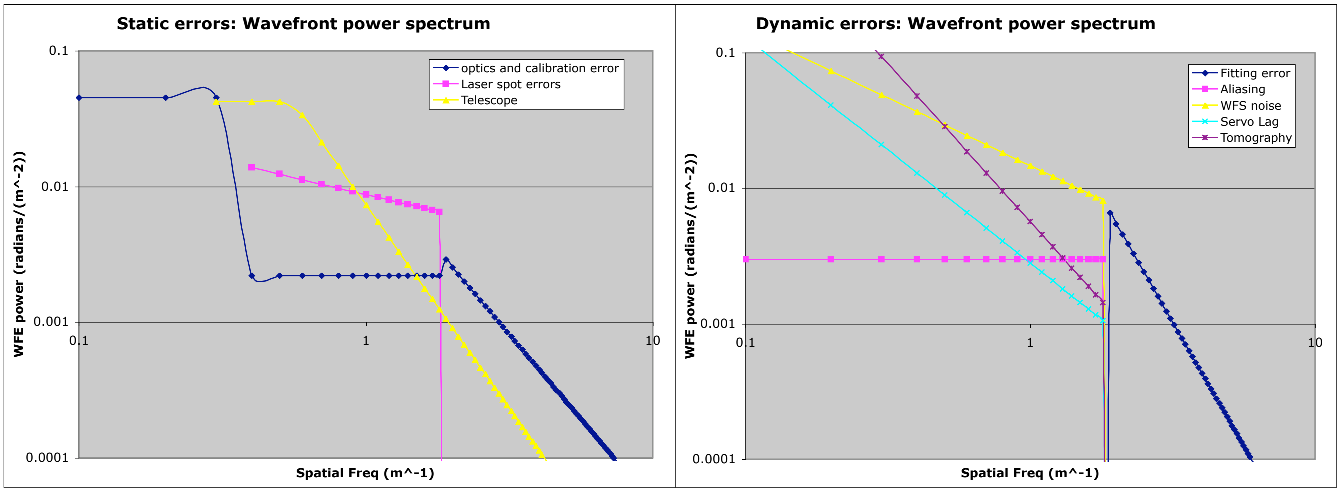

Figure 15: Dynamic and static wavefront error PSDs as currently implemented in the contrast spread sheet tool.

have associated Fried parameters r_{0l} and wind velocities $\mathbf{v}_l$. The WFS integration time and additional delay are t_i and t_d, and the von Karman outer scale L_0 enters in to the frequency cut-off $f_0 = 1/L_0$.

A.2.1 Servo-lag

Servo-lag, or bandwidth errors, arise from the finite integration time of the WFS and additional latency in the control loop (read-out, centroid calculations, wavefront reconstruction). The form given below implements a simple closed loop model for and integrating controller with gain g:

$$\Phi_{servo}(\mathbf{f}) = \frac{0.023}{(f^2 + f_0^2)} \times \sum_{l=1}^{N_l} r_{0l}^{-5/3} \left|\Gamma_l(\mathbf{f})\right|^2, \tag{5}$$

where

$$\Gamma_l(\mathbf{f}) = 1 - \mathrm{sinc}(\mathbf{f} \cdot \mathbf{v}_l t_i) \exp(2\pi i \mathbf{f} \cdot \mathbf{v}_l t_d) \times \frac{(e^{ib_l} - a)(1-a)}{1 - 2a\cos b_l + a^2} \tag{6}$$

with a and b_l defined as $a = 1 - g$ and $b_l = 2\pi \mathbf{f} \cdot \mathbf{v}_l t_i$. An example of the servo-lag PSD is plotted in Fig. 16 (upper right panel). The dashed orange line is a power-law curve-fit to the high-frequency part of the PSD. Most of the PSD is well approximated by a $f^{-5/3}$ power law, which becomes broken at very low spatial frequencies. Currently the contrast tool implements servo-lag as a pure -5/3 power law.

A.2.2 Noise

Of interest for high-contrast imaging is both the propagation of WFS photon and electrical noise into wavefront errors, and image speckle noise. The formula below only addresses the former, and results in a f^{-2} power law multiplied by the input noise PSD Φ_ν:

$$\Phi_{noise}(\mathbf{f}) = \frac{g}{2-g} \times \frac{\Phi_\nu(\mathbf{f})}{\mathrm{sinc}^2(\mathbf{f}d)} \left(\frac{1}{f_x^2} + \frac{1}{f_y^2}\right). \tag{7}$$

If the input is white noise, the classical f^{-2} power law is retained over most of the range, as shown in the lower left panel of Fig. 16. In the contrast tool, noise is currently modeled as f^{-1} [motivation?]

A.2.3 Spatial aliasing

Spatial aliasing errors arises in the WFS from high-spatial-frequency turbulence above the cut-off of the AO system that become measured, erroneously, as a lower frequency contribution. This error is usually not large in terms of

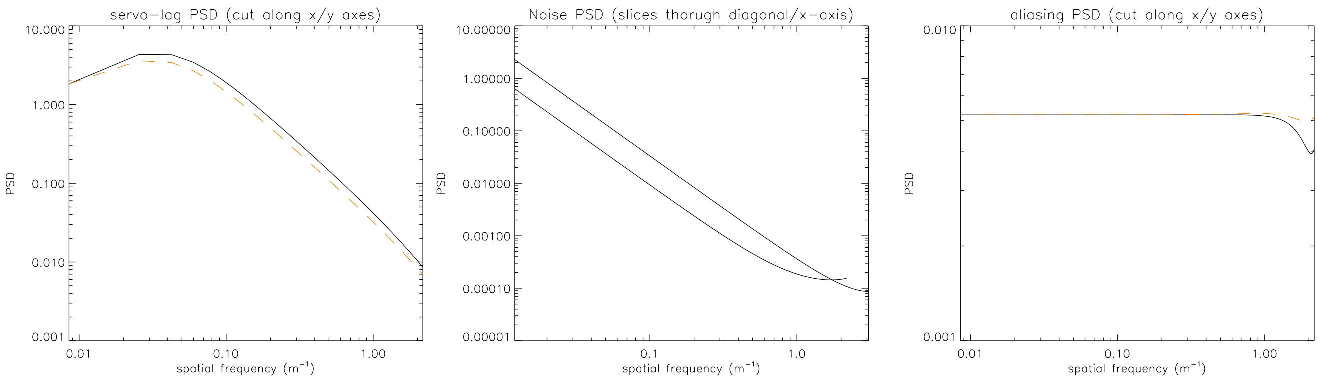

Figure 16: Cross-sections of spatial frequency PSDs from analytical models.

its contribution to the total wavefront error (approximately one third of the fitting error), but it contributes evenly to the middle-frequency range that is critical for high-contrast imaging. In NGS systems, aliasing can be reduced by spatially filtering the WFS beam, but currently it is unclear whether it will be possible to do the same for LGS systems. It was assumed in the contrast tool and numerical simulations that spatial filters may not be applied to reduce aliasing for NGAO. The closed-loop formula for spatial aliasing is given by

$$\Phi_{alias}(\mathbf{f}) = \frac{0.00575}{\mathrm{sinc}^2(\mathbf{f}d)} \times \sum_{\mathbf{m}\neq(0,0)} \frac{(\mathbf{f}^{-1}\cdot\mathbf{f}_m)^2\,\mathrm{sinc}^2(d\mathbf{f}_m)}{(|\mathbf{f}_m|^2+f_0^2)^{11/6}} \sum_{l=1}^{N_l} r_{0l}^{-5/3} \frac{g^2\,\mathrm{sinc}^2(\mathbf{f}_m\cdot\mathbf{v}_l t_i)}{1-2a\cos b_l + a^2}, \tag{8}$$

where $a = 1 - g$ and $b_l = 2\pi\mathbf{f}_m \cdot \mathbf{v}_l t_i$, and $\mathbf{f}_m = (f_x - m/d, f_y = n/d)$. As is seen in the lower right panel of Fig. 16, WFS spatial aliasing is very nearly flat from the center out to close to the cut-off frequency. It may for all practical purposes (and with adequate realism) be modeled as flat in the contrast tool, as it currently is.

A.2.4 Tomography error

The tomography error in a multi-LGS AO system does not have a simple analytical expression like the above terms that would allow us to compute it easily. It is currently modeled in the contrast tool as a f^{-2} power law, with the exponent adjustable should better estimations materialize. One experimental method was attempted (notes on Twiki, see Appendix B) to extract the PSD of tomography from a simulated PSF that contained only tomography errors and the effect of the telescope aperture by deconvolution. The tentative result is shown in Fig. 18, which attempted this deconvolution for two different LGS asterisms (5a and 8a in the terminology of KAON429) and for PSFs evaluated at a number of different sky positions, thereby containing varying mixtures of tomography/anisoplanatism errors. The on-axis case which most closely resembles what we wish to model as tomograpy error in the contrast tool, was found to have a slope roughly equal to a f^{-2} power law (-1.8), growing steeper as the PSF was further removed from the central axis (i.e. more anisoplanatism). The ripples observed are most likely residual effects of the finite aperture, which could not be deconvolved completely.

A.3 What is currently not modeled or well understood

The simulation code does not currently implement non-common path errors, but it would be possible to include in a modified version of the code. This mechanism would allow a range of different residual static aberrations from different sources to be analyzed by the same method. The character and significance of LGS related quasi-static aberrations also needs to be defined, investigated and understood.

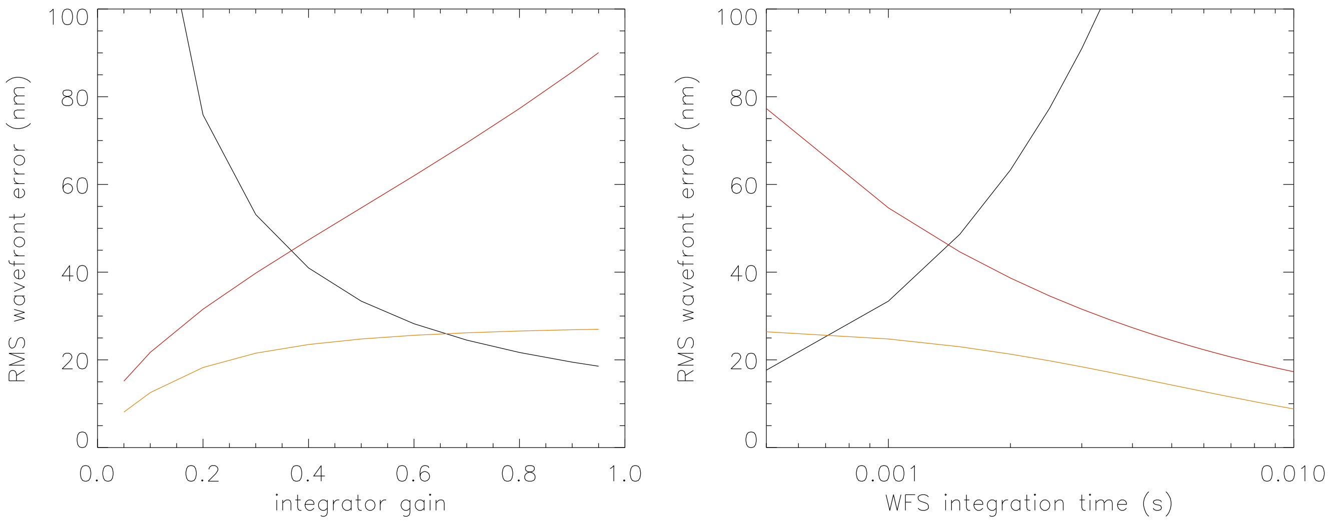

Figure 17: Servo-lag (black line), noise (red) and aliasing (orange) wavefront errors as functions of the integrator gain g (left) and the WFS integration time t_i (right). In a far-flung future, it would be great if the contrast tool implemented these closed-loop versions of the servo-lag, noise and aliasing errors, with a frame rate optimization mechanism.

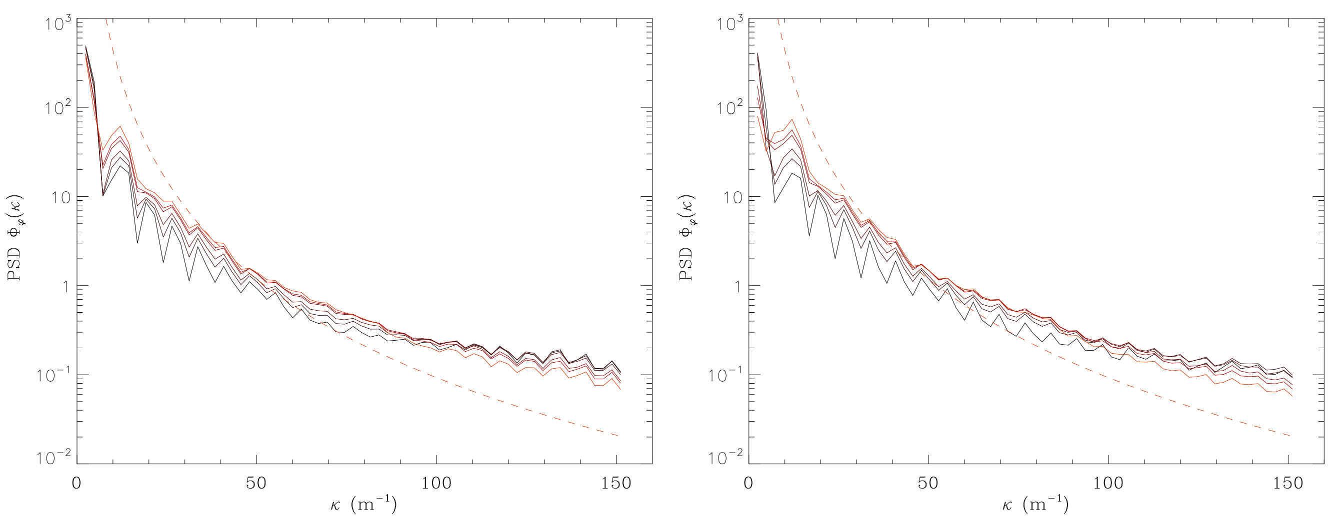

Figure 18: Azimuthally averaged residual phase power spectrum Φ_φ for asterism 5a (left) and 8a (right) computed by the Gaussian ML deconvolution method 2 (see NGAO note on Twiki). The dashed curve shows a $-11/3$ power law for comparison (not scaled to a physically phase variance).

B Applicable documents

- Photometric system: NGAO_Perf_Budget_Template.xls
  `http://www.oir.caltech.edu/twiki_oir/bin/view.cgi/Keck/NGAO/NGAOTemplates`
- Analytical evaluations of closed-loop adaptive optics spatial power spectral densities
  `http://www.oir.caltech.edu/twiki_oir/pub/Keck/NGAO/HighContrastBudget/aoclpsd.pdf`
- Estimating the spatial power spectrum of residual wavefront errors from adaptive optics simulations
  `http://www.oir.caltech.edu/twiki_oir/pub/Keck/NGAO/HighContrastBudget/tomoPSD.pdf`
- Yorick Adaptive Optics package (open source): `http://www.maumae.net/yao/aosimul.html`
- KAONs (Keck Adaptive Optics Notes):
  `http://www.oir.caltech.edu/twiki_oir/bin/view.cgi/Keck/NGAO/NewKAONs`
  - KAON 303 : Mauna Kea Atmospheric Parameters (CN-M1,M2,M3 models)
  - KAON 455 : Science Case Requirements Document v1.0
  - KAON 456 : System Requirements Document v1.10
  - KAON 461 : Wavefront Error Budget Predictions & Measured Performance for Current & Upgraded KAO
  - KAON 468 : An Algorithm for Reconstruction of Keck Telescope Segment Figures
  - KAON 471 : NGAO Wavefront Error and Ensquared Energy Budgets
  - KAON 492 : NGAO null-mode and quadratic mode tomography error

References

[1] J. W. Hardy. *Adaptive optics for Astronomical Telescope.* Oxford University Press, 1998.

[2] L. Jolissaint, J.-P. Véran, and R. Conan. Analytical modeling of adaptive optics: foundations of the phase spatial power spectrum approach. *Journal of the Optical Society of America A*, 23:382–394, February 2006.

[3] F. J. Rigaut, J. Veran, and O. Lai. Analytical model for Shack-Hartmann-based adaptive optics systems. In Domenico Bonaccini and Robert K. Tyson, editors, *Adaptive Optical System Technologies*, volume 3353 of *Proc. SPIE*, pages 1038–1048, September 1998.

[4] A. Sivaramakrishnan, C. D. Koresko, R. B. Makidon, T. Berkefeld, and M. J. Kuchner. Ground-based Coronagraphy with High-order Adaptive Optics. *Astrophys. J.*, 552:397–408, May 2001.